Supplementary Material

Economic feasibility of green hydrogen production by water electrolysis using wind and geothermal energy resources in Asal-Ghoubbet Rift (Republic of Djibouti): A comparative evaluation

Mohamed Osman Awaleh[1*], Abdi-Basid Adan[1*], Omar Assowe Dabar[1*], Mohamed Jalludin[1], Moussa Mahdi Ahmed[1] and Ismael Abdillahi Guirreh[2]

[1]Institut des Sciences de la Terre. Centre d'Etudes et de Recherches de Djibouti (CERD), Route de l'aeroport, B.P. 486. Djibouti - ville, République de Djibouti ; mohamed.jalludin@gmail.com (M.J) ; moussa.mahdi@chemist.com (M.M.A)

[2]Université de Djibouti, Croisement RN2-RN5, B.P. 1904. Balbala, République de Djibouti ; ismael.abdillahi@gmail.com (I.A.G.)

*Correspondence: awaleh@gmail.com; Abdi-Basid@outlook.com; Assowe440@gmail.com

S1. Methodology

S1.1. Weibull distribution

S1.1.1 Maximum likelihood method

This method determines the shape factor and scale factor after extensive iterations. The method of Maximum Likelihood is the most popular technique to perform the estimation of the Weibull parameters, especially for time series of wind data. In this method, the parameters k and c are computed using the equations below [1]:

$$k = \left[\frac{\sum_{i=1}^{n} v_i^k \ln(v_i)}{\sum_{i=1}^{n} v_i^k} - \frac{\sum_{i=1}^{n} \ln(v_i)}{n} \right]^{-1} \tag{1}$$

$$c = \left[\frac{1}{n} \sum_{i=1}^{n} v_i^k \right]^{\frac{1}{k}} \tag{2}$$

Where v_i is the wind speed in time i and n is the number of non-zero elements.

S1.1.2 W AsP method

The WAsP method has a requirement that the Weibull distribution should fit the measured wind speed data [2]. The WAsP method does not attempt to directly fit the measured frequency histogram, but has the two following requirements; (i) The mean power density of the fitted Weibull distribution must be equal to that of the observed distribution and, (ii) The frequencies of values above the mean observed wind speed must correspond to the fitted Weibull distribution as for the observed distribution [2].

$$c = \left(\frac{\sum_{i=1}^{n} v_i^3}{n\Gamma\left(\frac{3}{k}+1\right)} \right)^{\frac{1}{3}} \tag{3}$$

In order to address the second aspect of this method, the shape factor k is computed form the Weibull cumulative distribution function F as [2]:

$$-\ln\left(1 - F(\overline{v})\right) = \left(\frac{\overline{v}}{c}\right)^k \tag{4}$$

S1.1.3 Moment method

As the maximum likelihood method, the moment method estimates the shape (k) and the scale (c) parameters through an iterative resolution of Eq. (5) and Eq. (6) [3]:

$$\bar{v} = c\,\Gamma\left(1 + \frac{1}{k}\right) \tag{5}$$

$$\sigma_v = c\left[\Gamma\left(1 + \frac{2}{k}\right) - \Gamma^2\left(1 + \frac{1}{k}\right)\right]^{\frac{1}{2}} \tag{6}$$

Where Γ, $\bar{v}$ and σ_v are respectively the gamma function, mean and standard deviation of the wind speed data. The Gamma function given by [3]:

$$\Gamma = \int_{t=0}^{t=\infty} t^{x-1} e^{-t} dt \tag{7}$$

S1.1.4 Empirical method of Jestus

This method is proposed by Jestus el al. [4] to find the (k) and (c) parameters if the mean wind speed v and standard deviation σ_v are available. This empirical method is a particular case of the moment method. The used empirical equations use the following equations to estimate k and c [5].

$$k = \left(\frac{\sigma_v}{\overline{v}}\right)^{-1.086} \qquad 1 \le k \le 10 \tag{8}$$

$$c = \frac{\overline{v}}{\Gamma\left(1 + \frac{1}{k}\right)} \tag{9}$$

S1.2 Performance analysis of Weibull fit methods

The accuracy of the four fitting methods for the estimation of Weibull parameters mentioned above was evaluated by the goodness of the fit statistics of coefficient of determination (R^2); the root means square deviation (RMSE) and the mean absolute error (MAE). The first statistics test (i.e., R^2) studies the linear relationship between the observed wind data and the estimated with the Weibull function. R^2 has a valued in the range 0 and 1. The Weibull fit model with the highest R^2, switch to the best estimated model of the measured wind speed data. Mathematically, the coefficient of determination is defined as follows [6]:

$$R^2 = \frac{\sum_{i=1}^n (y_i - z_i)^2 - \sum_{i=1}^n (y_i - x_i)^2}{\sum_{i=1}^n (y_i - z_i)^2} \tag{10}$$

The root mean square error (RMSE) assesses the accuracy of the fitting method used by comparing the difference between the distribution of the Weibull function and the observed wind data. The Weibull fit model with the smallest RMSE is more accurate and provide the best estimates of the parameters of the Weibull distribution function. The root mean square error can be calculated with the following expression [6]:

$$RMSE = \left[\frac{1}{N} \sum_{i=1}^n (y_i - x_i)^2 \right]^{1/2} \tag{11}$$

The mean absolute error (MAE) is the average in absolute value of the discrepancy between the observations and the predicted from the Weibull density. MAE always has a positive value and indicates a higher accurate of the Weibull fit model, when its value is small. The mean absolute error can be calculated with the following expression [7]:

$$MAE = \frac{1}{N} \sum_{i=1}^n |y_i - x_i| \tag{12}$$

Where N is the number of observations, y_i is the frequency of the measured data, x_i is the Weibull distribution model, z_i is the average of the wind speeds from observation.

S2. Geothermal resources assessment

S2.1. USGS volumetric method

The volumetric method is one of the most widely used methods to quantify resource capacity in a geothermal reservoir [8]. The potential geothermal energy capacity in a reservoir (MWe) can be evaluated with the following mathematical expression [9]:

$$E_{GT} = E_R + E_W \tag{13}$$

$$E_R = A_r.H_r \left(\rho_R.C_R \times (1 - \emptyset) \times (T_i - T_f) \right) \tag{14}$$

$$E_W = A_r.H_r \left(\rho_W.C_W \times \emptyset (T_i - T_f) \right) \tag{15}$$

Where E_{GT} thermal energy in the reservoir in (MJ), L_t geothermal plant life. L_f is the load factor; R_f is the recovery factor and C_e is the conversion efficiency. $\rho_R.C_R$ are Specific heat and rock density in reservoir; $\rho_W.C_W$ are Specific heat and fluid density rock. $\emptyset$ is the porosity. A_r is the area of reservoir and H_r is the thickness reservoir. T_i and T_{if} represent the reference temperature and cut off temperature, respectively.

Moreover, the volumetric method in combination with the Monte Carlo method is used to minimize the parameter uncertainty. Some of probability distributions of triangular; lognormal and uniform are required [10]. More runs of Simulation modeling allow accurate results. Three frequencies are used for stochastic evaluation of reservoir capacity: the case of 90% (i.e., proven capacity); 50% (proven and probable capacity) and 10% (proven, probable and possible capacity) [11]. Analyses of the Sensitivity of the input parameters quantify the variability of parameter uncertainties and assessment of the impact of each reservoir parameter on the estimation of geothermal reservoir capacity.

S2.2. Thermodynamic assessment

The thermodynamic performances of single flash and dry steam are evaluated in terms of energy and exergy, according to the first and second laws of thermodynamics. Throughout this analysis in our study, the following assumptions are made accordingly:

(i) The system operates in a steady state [12]. (ii) Potential and kinetic energies are considered to be insignificant [13]. (iii) Ambient temperature and pressure are assumed to be 298.15 K and 1013 kPa [14]. When conserving mass and energy in an irreversible process, entropy is generated and exergy is destroyed. The mass, energy and exergy balances for any steady-state control volume with negligible changes in kinetic and potential energy are given with the following mathematical equations [15]:

$$\sum \dot{m}_\iota = \sum \dot{m}_e \tag{16}$$

$$\dot{Q} - \dot{W} = \sum \dot{m}_e h_e - \sum \dot{m}_\iota h_i \tag{17}$$

$$\dot{E}_Q - \dot{W} = \sum \dot{m}_e e_e - \sum \dot{m}_\iota e_i + \dot{E}_D \tag{18}$$

where $\dot{Q}$ and $\dot{W}$ are the net inputs of heat and work, $\dot{m}$ is the mass flow rate of the fluid flow, h is the enthalpy, e is the specific flow rate of the exergy, $\dot{E}_Q$ is the rate of exergy transfer through heat, $\dot{E}_D$ is the rate of exergy destruction, and the indices i and e represent the input and output states. The specific flux exergy and the total exergy rate can be calculated as follows [15]:

$$e = (h - h_0) - T_0(s - s_0) \tag{19}$$
$$\dot{E} = \dot{m}(e) \tag{20}$$

Where s is entropy, T_0 is the dead state temperature (25°C), and the subscripts 0 stands for the restricted dead state for geofluid.

The maximum specific work that can be achieved by a geothermal power plant using geothermal water at Ts in an environment at T₀ can be calculated with the following expression:

$$W_{max} = (h_s - h_0) - T_0(S_s - S_0) \tag{21}$$

Where hs and ss are enthalpy and entropy of geothermal water, respectively.

The energy and exergy efficiencies are defined with the following mathematical equations:

$$\eta_{th} = \left(\frac{energy\ in\ kth\ component}{total\ energy\ input}\right) \tag{22}$$

$$\eta_{th} = \left(\frac{exergy\ in\ kth\ component}{total\ energy\ input}\right) \tag{23}$$

S3. Production wind and geothermal decline

Ageing production capacity is an inevitable reality for all types of turbine. This is characterized by the reduction of the initial production performance. In this section, the declination rate of a wind turbine and a geothermal well are evaluated. Indeed, the load factor of a wind turbine, which decreases with age at an annual rate of 1.6% ± 0.2% [16, 17]. However, in the geothermal case, a typical harmonic decline rate of 5% can be considered per year for geothermal

well [15]. To calculate the annual potential of geothermal well in a given period and the annual rate of decline for the year k, the following expressions can be considered [18]:

$$W = \frac{W_i}{1 + D_{i,k}} \tag{24}$$

$$D = \frac{D_i}{1 + D_{i,t}} \tag{25}$$

In the previous equation, Wi is the initial production rate, W is the production rate at time t and Di is the initial decline rate, W is the power produced by the well in year k. Additionally, an increase in installed capacity production leads to an increase in the reduction rate. This relationship can be evaluated with the following mathematical equation [18]:

$$D_i' = \left(\frac{W_i'}{W_i}\right) \times \left(\frac{\ln(W_i')}{\ln(W_i)}\right) \times D_i \tag{26}$$

Here, D_i is the initial annual harmonic reduction rate of productivity when the total the production rate is W_i and D_i' are the initial annual rate of reduction of harmonics when the total production the rate is changed to W_i'. The number of years during which the installed installation can be maintained without any additional well drilling has been proposed by Ref. [18] as follows:

$$t_c = \frac{1}{D_i}\left[\left(\frac{W_i\, N_{wi}}{(1 + r/100) \times P}\right) - 1\right] \tag{27}$$

Where D_i is the initial annual harmonic decline rate. W_i is the initial productivity per well (MW), N_{wi} is the initial number of wells, (including at least one stand-by well), P is the plant capacity (MWe), and r is the minimum reserve production required capacity.

S4. Green house assessment of wind and geothermal energies

S4.1. Evaluation of CO₂ reduction from wind energy

In order to reduce the environment impact of the Carbone dioxide (CO_2) emissions with the deployment of renewable energy, the electricity from wind and geothermal source are compared to the fossil fuel power plant performance. For this purpose, the IPCC recommended an emission factor from fossil fuel per KWh at 77 tons CO₂/TJ (equivalent of 0.277 kCO₂/kWh) [19]. The annual amount of CO₂ saved can be calculated as fellow [20].

$$CO_{2\ emission\ reduction} = E_{out}(kWh/year) \times 0.277\ (kCO_2/kWh) \tag{28}$$

S4.2. Exergoenvironmental of geothermal energy assessment

The potential decrease of greenhouse gas emissions with the geothermal energy is carrying out on the result of thermodynamics. Indeed, the exergo environmental impact factor represents how well a geothermal power station is harmful to the environment and the impact index factor and the improvement of this factor evaluate how much geothermal power plant damage the environmental. The exergoenvironmental analysis is evaluated with the following equations [21]:

$$f_{ex} = \frac{\dot{E}_{x_{D,Tot}}}{\dot{E}_{x_{in}}} \tag{29}$$

$$\theta_{ex} = \frac{100 \times f_{ex}}{\eta_{II}} \tag{30}$$

$$\theta_{ex'} = \frac{1}{\theta_{ex}} \tag{31}$$

Where f_{ex} is the impact factor; $\dot{E}_{x_{D,Tot}}$ and $\dot{E}_{x_{in}}$ represented the total exergy destruction and the exergy entering in KW of the geothermal power plant. θ_{ex} is the impact index factor; η_{II} is the exergy efficiency of the power plant and $\theta_{ex'}$ is the improvement of impact index factor.
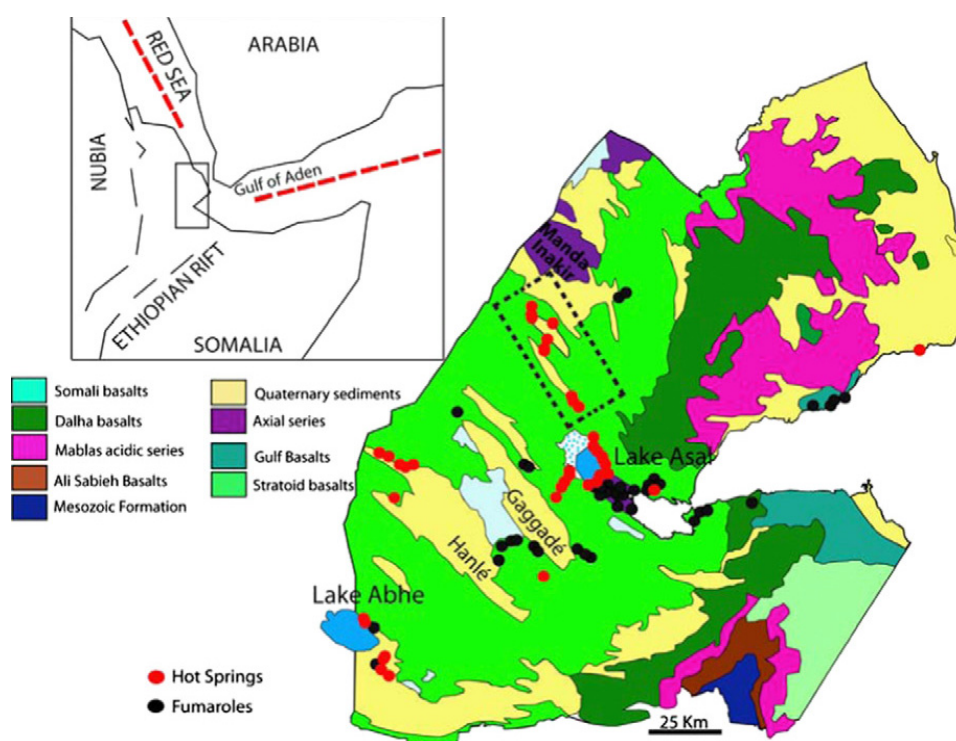
Figure S1. A schematic geological map of the Republic of Djibouti (SE Afar Rift) and hydrothermal activity of the Republic of Djibouti (Awaleh et al., 2017). In the inset: schematic map of the Afar Depression with the location of Djibouti (black rectangle) [22].
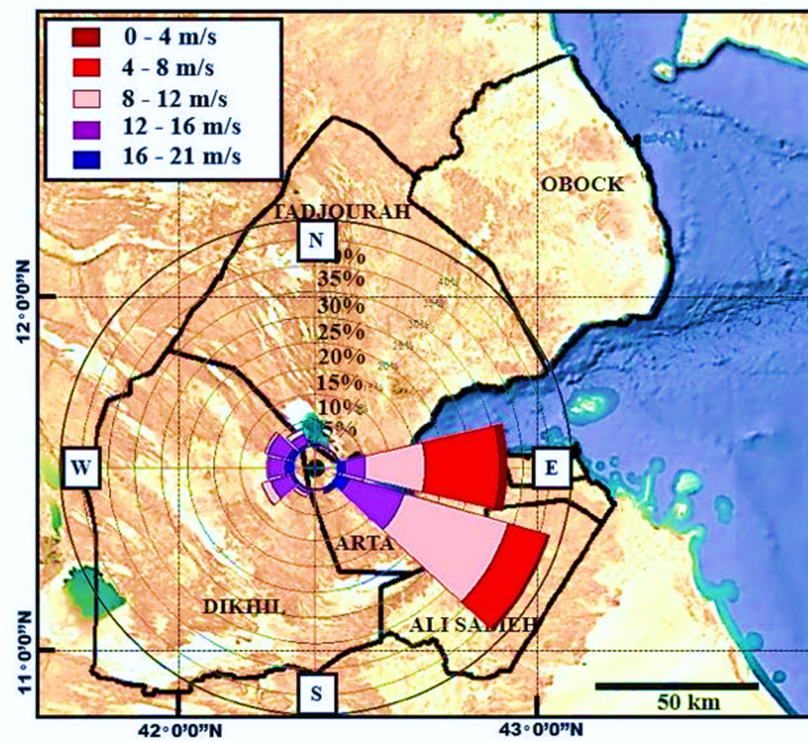
S2. Results

Figure S2. Annual wind direction for Ghoubbet at level of 60 m of year 2015

Table S1. Different size of water electrolysis model (0.4 to 800 Nm³/h [23]).

	Designate Electroyzer	Rated power (KW)	Energy required (KWh/kg)	Efficiency of Electrolyzer (%)	Operation time per day (hr)	Efficiency of rectifier (%)	Lifespan (yr)	References
SMALL			Electrolyser System Range of 0.4 to 20 Nm3/h [23]					
Polymer/Proton Electrolyte Membrane Electrolysis (PEME)	**PEMEs**	7.2	80.10	41.61	24	90	7 (Electrolyzer) / 10 (Rectifier)	[24]
Alkaline Bipolar Electrolysis (AWE)	**AWEs**	80	55.6	70.80	24	90	7 (Electrolyzer) / 10 (Rectifier)	[24]
MEDUIM			Electrolyser System Range of 20 to 100 Nm3/h [23]					
Polymer/Proton Electrolyte Membrane Electrolysis (PEME)	**PEMEm**	185	54	61.72	24	90	20(Electrolyzer) / 10 (Rectifier)	[24]
Alkaline Bipolar Electrolysis (AWE)	**AWEm**	312	57.9	68.10	24	90	15 (Electrolyzer) / 10 (Rectifier)	[26]
LARGE			Electrolyser System Range of 100 to 800 Nm3/h [23]					
Polymer/Proton Electrolyte Membrane Electrolysis (PEME)	**PEMEl**	1500	83	40.16	24	90	15-20 (Electrolyzer) / 10 (Rectifier)	[25]
Alkaline Bipolar Electrolysis (AWE)	**AWEl**	1000	42	79.36	24	90	15 (Electrolyzer) / 10 (Rectifier)	[26]
High-Temperature electrolyzer unit (HTE)	- -	- -	23.57	94	24	90	10	[27,28]

Table S2. Important parameters for the major stages of a single flash Power Plant (see figure 5).

Sate	Pressure (kPa)	Temperature (°C)	Enthalpy (kJ/kg)	Entropy (kJ/kg K)	Mass flow (kg/s)	Energy (kW)	Energy (%)	Exergy (kW)	Exergy (%)
0	100	25							
1	9211.55	306	2739.36	5.67	40.00	109574.49	78.83	4315412.15	62.88
2	872.94	174	2752.18	6.63	40.00	110087.10	79.20	4324388.39	63.02
3	872.94	174	2752.18	6.63	12.51	34430.27	24.77	405991.71	5.92
4	14.55	53	2596.96	8.02	12.51	32488.50	23.37	376523.03	5.49
5	14.55	53	2596.96	8.02	12.51	32488.50	23.37	376523.03	5.49
6	872.94	174	2752.18	6.63	12.51	34430.27	24.77	405991.71	5.92
7	100	25	2546.50	8.56	12.51	31857.20	22.92	366611.62	5.34
8	100	35	2564.60	8.35	40.00	102584.00	73.80	4003777.90	58.34
9	17.74	55	2604.22	7.95	12.51	32579.28	23.44	377915.79	5.51
10	17.74	55	2604.22	7.95	12.51	32579.28	23.44	377915.79	5.51

Table S3. Important parameters for the major stages of a dry steam power plant (see figure 4)

Sate	Pressure (kPa)	Temperature (°C)	Enthalpy (kJ/kg)	Entropy (kJ/kg K)	Mass flow (kg/s)	Energy (kW)	Energy (%)	Exergy (kW)	Exergy (%)
0	100	25	2546.50	8.56					
1	9211.55	306	2739.36	5.67	40	109574.49	78.83	4315412.15	62.88
2	14.55	53.22	2596.96	8.02	40	103878.50	74.74	4059492.41	59.16
3	14.55	53.22	2596.96	8.02	40	103878.50	74.74	4059492.41	59.16
4	100	25	2546.50	8.56	12.51	31857.20	22.92	366623.93	5.34
5	100	35	2564.60	8.35	40	102584.00	73.80	4003757.63	58.34

Table S4. Statistics summary of wind speed at level of 80 m of Ghoubbet.

Statistics parameters at level of 80 m	Values
Mean wind speed (m/s)	10.00
Standard Deviation	4.02
Minimum Wind speed (m/s)	0.42
Maximum wind speed (ms/)	21.108
Power density (W/m²)	904.455
Wind shear (60-80m)	0.2048
Skewness coefficient	-0.140
Kurtosis coefficient	-0.633

Table S5. Characteristics of the different wind turbine models considered in this study and the calculated Annual energy production and the capacity factor [29].

WIND TURBINE	Designate Turbine	Rated Power (kW)	Cut-in speed (m/s)	Rated speed (m/s)	Cut-out speed (m/s)	Hub Height (m)	Lifetime (yr)	Cf (%)	Eout (MWh/yr)
Neg Micon NM60/1000	T1	1000	3	16	20	70/80	20	0.342841	3003.28
ELKRAFT Avedøre 1MW	T2	1000	4	15	25	55	20	0.39241	3437.55
Suzlon S.64-1000	T3	1000	3	11	25	65	20	0.63692	5579.46
Goldwind GW 62/1200	T4	1200	3	12.5	25	69/85	20	0.54400	5718.50
DeWind D6 64/1250	T5	1250	2.5	12.3	25	68/91.5	20	0.56001	6132.12
Suzlon S.66-1250	T6	1250	4	12	20	74.5	20	0.55427	6069.26
Goldwind GW 87/1500	T7	1500	3	9.9	22	75/85	20	0.70216	9226.37
GE 1.5sle	T8	1500	3.5	12	25	61.4/64.7/80/85	20	0.56973	7486.22
GE 1.6-82.5	T9	1600	3.5	10	25	65/80/100	20	0.69259	9707.33
ECO 80/1670	T10	1670	3	25	34	60/70/80	20	0.11466	1677.45
Vestas V82-1.65	T11	1650	2.5	13	32	59-108	20	0.51750	7479.94
Gamesa G66	T12	1650	4	15	25	60/78	20	0.39241	5671.96
Envision EN106-1.8	T13	1800	3	9.5	20	80/90/100	20	0.71899	11337.07
Vestas V100-1.8	T14	1800	3	12	20	80/95/120	20	0.56563	8918.84
GE 1.85 - 82.5	T15	1850	3	13	25	65/80/100	20	0.51374	8325.62
GE 1.85 - 87	T16	1850	3	12.5	25	80	20	0.54400	8 816.02
Gamesa G80	T17	2000	3.5	12	25	60/67/78/100	20	0.56973	9981.62
Vestas V110	T18	2000	3	11.5	20	80/95/125	20	0.59668	10453.87
Gamesa G114-2.1MW	T19	2100	1	11.5	25	80/93/106/125	20	0.61563	11325.04
Avantis AV 1010	T20	2300	3	11.2	25	99	20	0.62449	12582.22
Senvion 2.3M120	T21	2330	3	12	20	90/120	20	0.56563	11544.94
Yinhe GX103-2.5MW	T22	2500	3	7.5	25	80	20	0.83575	18302.85
Kenersys K100 2.5MW	T23	2500	3	14	25	85/100/135	20	0.45549	9975.21
Yinhe GX93-2.5MW	T24	2500	3	8,5	25	80	20	0.78469	17184.61
Yinhe GX113-2.5MW	T25	2500	3	7	20	88.3	20	**0.84962**	**18606.64**

Gamesa G114-2.625MW	T26	2630	2	11	25	68/80/93/125	20	0.64400	14837.00
Alstom ECO 122/2700	T27	2700	3	10	34	89	20	0.69853	16521.71
Dongfang G3000-119	T28	3000	3	10.5	20	90 / site-specific	20	0.65871	17310.98
Enercon E-101	T29	3050	2	13	25	99/124/135/149	20	0.51986	13889.53
E-101 E2 3.050	T30	3050	2	13	34	74	20	0.52006	13894.97
General Electric GE 3.2s	T31	3200	3	14.3	25	100 - 140	20	0.43876	12299.24
General Electric GE3.2-130	T32	3200	2	12	25	85/110/134/155	20	0.58137	16296.83
Gamesa G132-3.3MW	T33	3300	2	10	25	84/97/114/134/site-specific	20	0.70586	20404.87
Goldwind GW 140/3400	T34	3400	2.5	10.1	20	100 / 110 / 120	20	0.68750	20476.47
Gamesa G132-3.465MW	T35	3470	3	11	25	84/97/114/134	20	0.63692	19360.73
Enercon E-101 E2 3.500	T36	3500	2	15	25	74	20	0.40645	12461.79
Goldwind GW 136/4200	T37	4200	2.5	11.2	25	100 / 110 / site-specific	20	0.62855	23125.65
Senvion 4.2M118	T38	4200	3	12.5	22	Site-specific	20	0.54180	19934.08
SWT DD /4300	T39	4300	3	15	25	115/135 m and site-specific	20	0.40129	15115.70
Goldwind GW 155/4500	T40	4500	2.5	10.8	26	95 / 110 / 140 / site-specific	20	0.65362	25765.82
ADWEN AD5-116	T41	5000	4	12.5	25	Site-specific	20	0.53306	23347.83
Sinovel SL5000/155	T42	5000	3.5	10	25	110	20	0.69259	30335.40

Table S6. Cost prospect of the wind-powered hydrogen production system in Ghoubbet without and with degradation rate.

| years	Capital investment (CI) in $	Annual operation and Maintenance cost (COM) in $	Present Value Cost (PVC) in $	Energy production (EWT) in kWh/yr	Energy production with degradation (EWT) in kWh/yr
0	5200000	0	5200000	0	0
1	0	316586,9938	316586.99	18606641.39	18606641.39
2	0	321241,4251	321241.43	18606641.39	18308935.13
3	0	325964,2854	325964.29	18606641.39	18015992.17
4	0	330756,5808	330756.58	18606641.39	17727736.29
5	0	335619,332	335619.33	18606641.39	17444092.51
6	0	340553,5749	340553.57	18606641.39	17164987.03
7	0	345560,3605	345560.36	18606641.39	16890347.24
8	0	350640,7555	350640.76	18606641.39	16620101.68
9	0	355795,8419	355795.84	18606641.39	16354180.05
10	0	361026,7179	361026.72	18606641.39	16092513.17
11	0	366334,4977	366334.50	18606641.39	15835032.96
12	0	371720,312	371720.31	18606641.39	15581672.44
13	0	377185,3081	377185.31	18606641.39	15332365.68
14	0	382730,6499	382730.65	18606641.39	15087047.83
15	0	388357,5189	388357.52	18606641.39	14845655.06
16	0	394067,1135	394067.11	18606641.39	14608124.58
17	0	399860,65	399860.65	18606641.39	14374394.59
18	0	405739,3626	405739.36	18606641.39	14144404.27
19	0	411704,5034	411704.50	18606641.39	13918093.80
20	0	417757,3431	417757.34	18606641.39	13695404.30
Total	**5200000**	7299203,127	**12499203.13**	**372132827.79**	**320647722.2**

Table S7. Electrolyzer performance analysis using wind energy [24-26, 29].

| Designate Electroyzer Model[1,2]	Rated power (KW)	Amount of H$_2$ (ton/yr)	Fresh water required (m³/yr)	Efficiency System (%)	Number of electrolyzer required	LCOH ($/kg)
PEME$_s$	7.2	209. 1	2326	10.38	315	7.187
AWE$_s$	80	301.1	3349.4	14.95	25	2.655
PEME$_m$	185	310.1	3450.3	15.40	13	0.680
AWE$_m$	312	289.5	3220.6	14.38	7	1.348
PEME$_l$	1500	201.8	2244.8	10.02	2	5.272
AWE$_l$	1000	398.7	4436.1	19.80	3	1.063

[1]PEME$_i$/AWE$_i$ (i.e : s for small size; m for medium; and l for large size) [2]Rectifier efficiency at 90%

The investment cost of the electrolyzer takes into account the capital cost, the annual operation and maintenance expenses, the replacement cost, the annual electricity consumption cost and the investment in raw material (desalinated water).
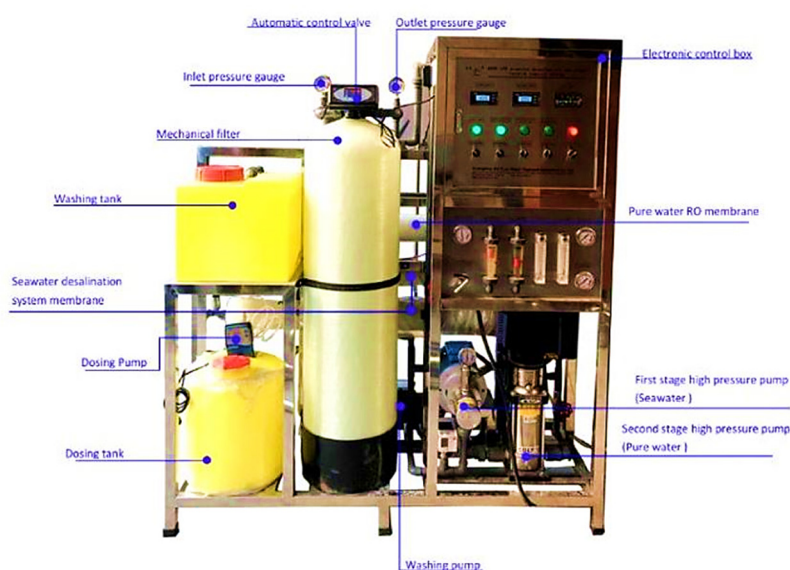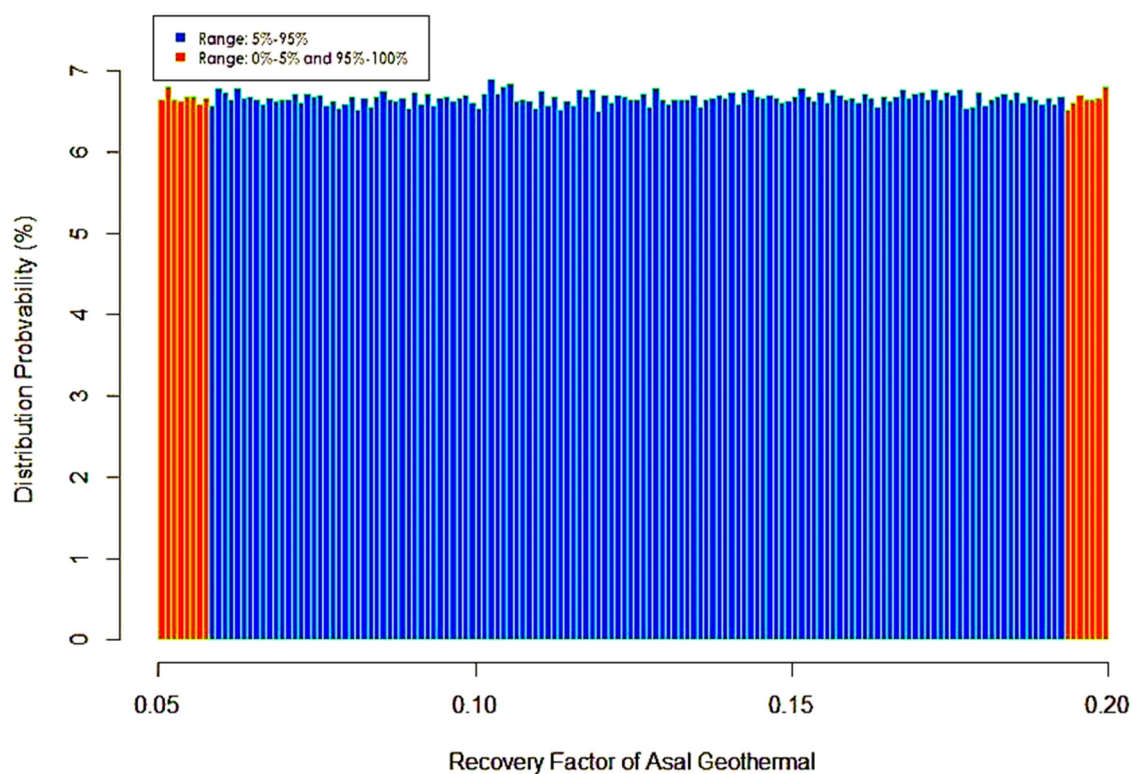

Figure S3. Different equipment of RO, Guangzhou Kai Yuan Water Treatment Equipment Co. Ltd [30].
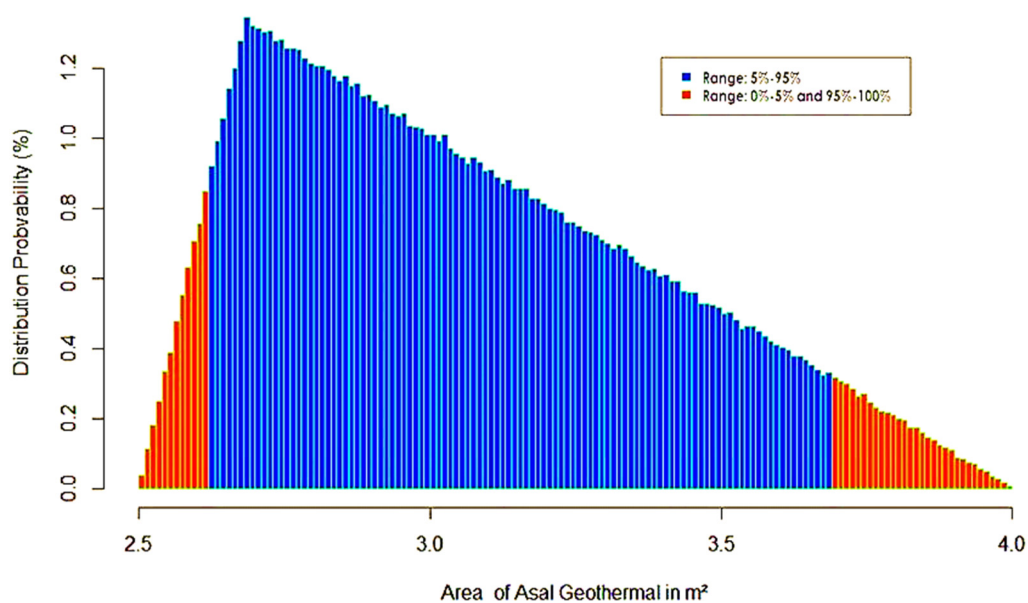
Figure S4. Probability distribution of Monte Carlo simulation of Area of Asal-Ghoubbet Rift in m².
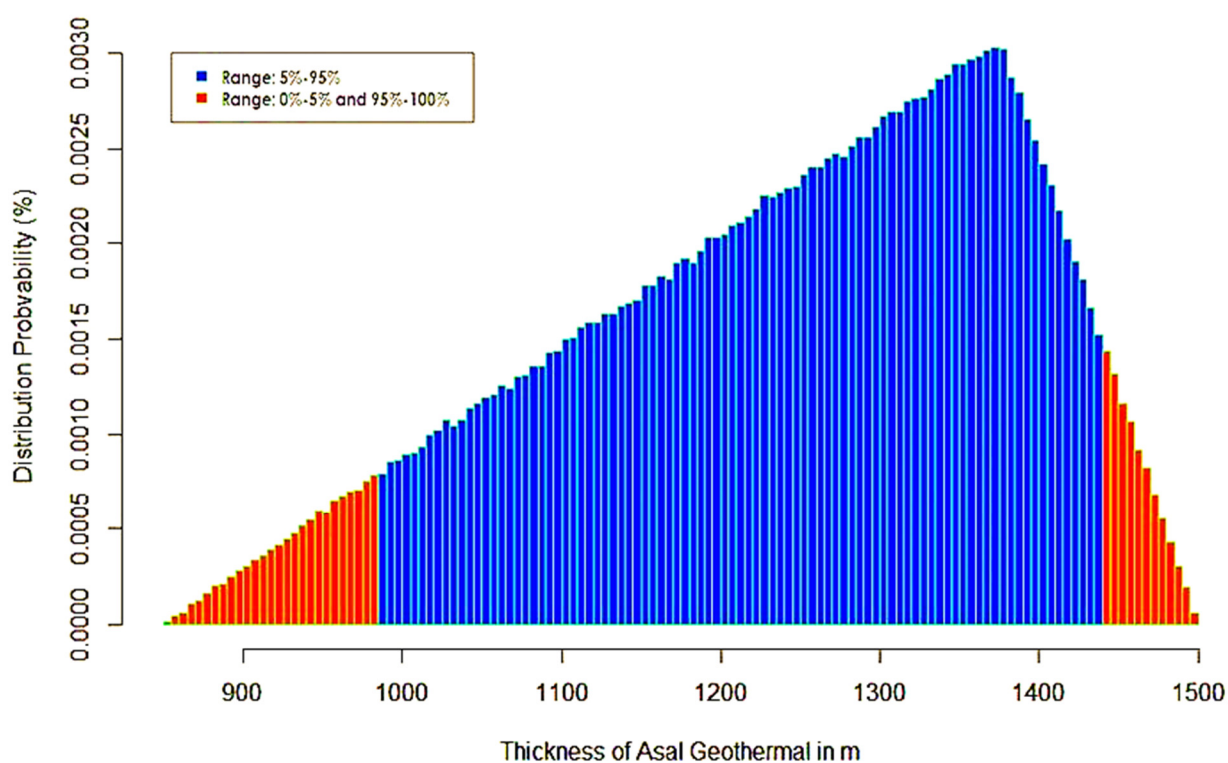
Figure S5. Probability distribution of Monte Carlo simulation of Thickness of Asal-Ghoubbet Rift.

Figure S6. Probability distribution of Monte Carlo simulation of Recovery Factor of Asal-Ghoubbet Rift.

Figure S7. Probability distribution of Monte Carlo simulation of Heat Specific of Rock of Asal-Ghoubbet Rift in J/kg°C.

Figure S8. Probability distribution of Monte Carlo simulation of Reference Temperature of Asal-Ghoubbet Rift in °C.
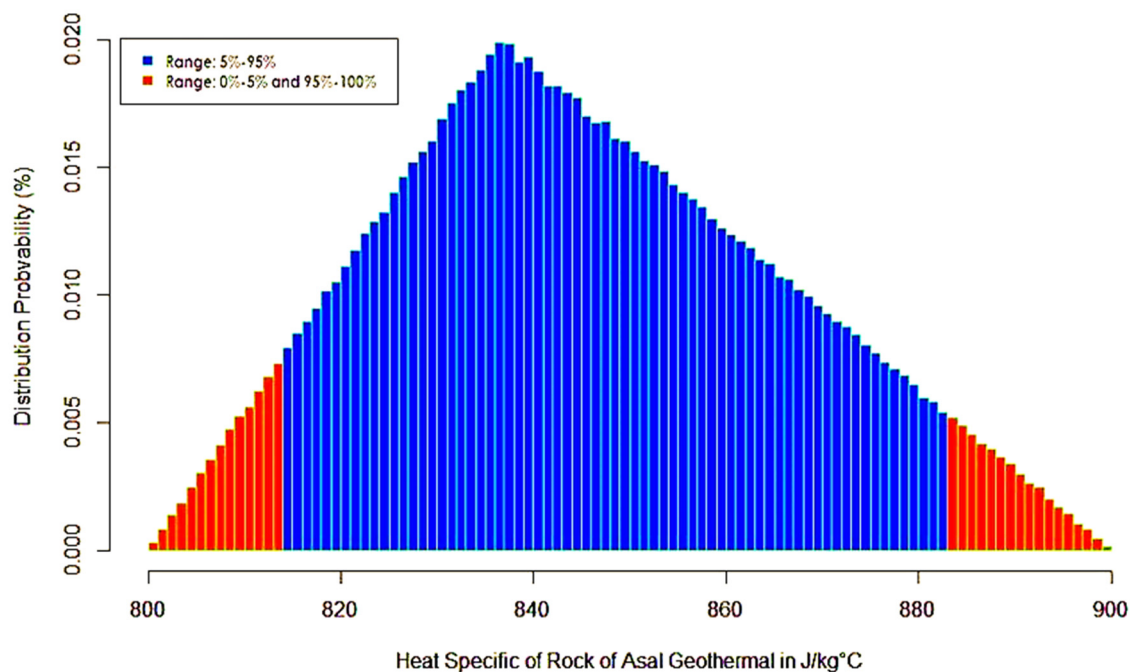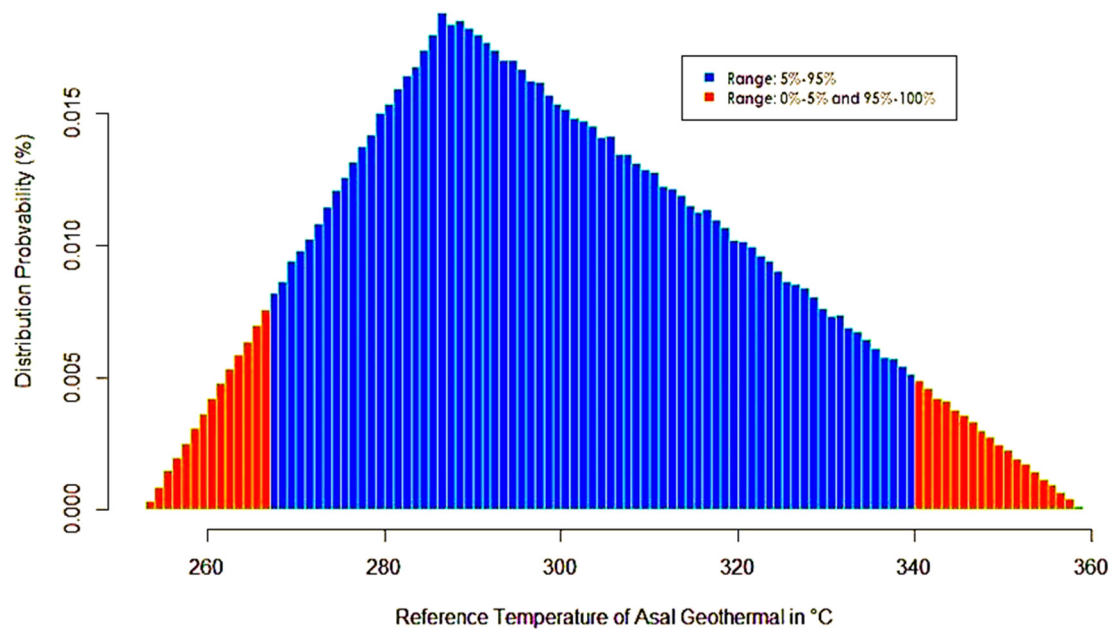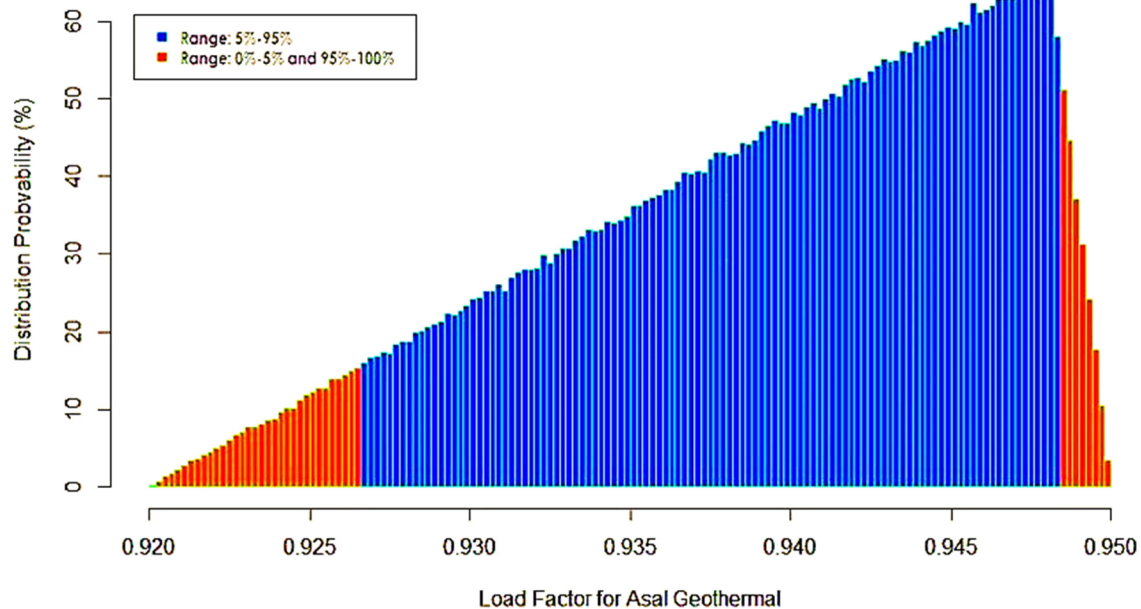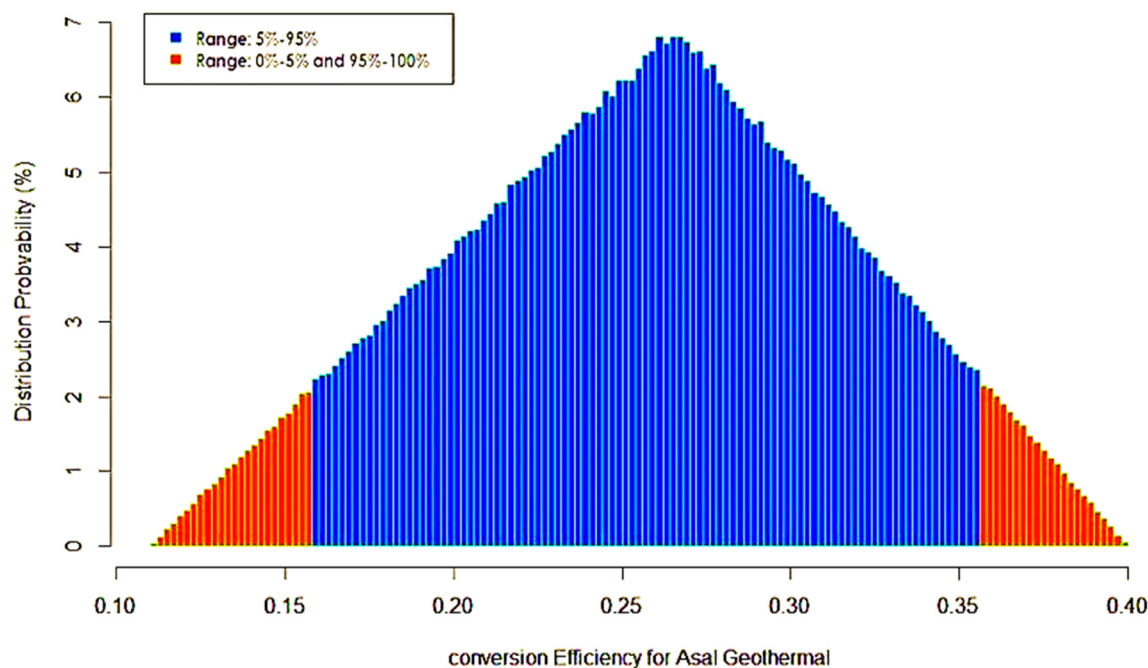

Figure S9. Probability distribution of Monte Carlo simulation of Load Factor of Asal-Ghoubbet Rift.

Figure S10. Probability distribution of Monte Carlo simulation of Conversion efficiency of Asal-Ghoubbet Rift.

Table S8. Most probable values and distributions for the parameters of USGS volumetric method for Asal-Ghoubbet Rift.

Entry Parameter of USGS	Unit	Average	Min	Max	Probability Distribution	Reference
Area of reservoir	km²	3.25	2.5	4	Triangular	[31-33]
Thickness of reservoir	m	1175	850	1500	Triangular	
Fluid Density	kg/m³	973	820	1126	Constant	[34, 35, 37, 38]
Fluid specific Heat Capacity	J/kg°C	4500	4200	4800	Constant	[42]
Rock Density	kg/m³	2500	2000	3000	Constant	[36, 39-41]
Rock Specific Heat Capacity	J/kg°C	875	850	900	Triangular	[32, 37, 48]
Reference Temperature	°C	306	253	359	Triangular	[43,33]
Final Temperature	°C	110	40	180	Constant	[44,45]
Pororsity	%	5.05	0.1	10	Lognormal	[31,41]
Recovery Factor	%	12.5	5	20	Uniform	[41,46]
Conversion Efficiency	%	25.5	11	40	Constant/ Triangular	[46,47]
Load Factor	%	93.5	92	95	Triangular	[46, 47, 10]
Life time	yr	25	/	/	Constant	[48]
Asal-Ghoubbet Rift Rock energy storage			1.546674.10e18 J	[90.38%]		67.18 MWe
Asal-Ghoubet Rift Fluid energy storage			1.646541.10e17 J	[9.62%]		7.15 MWe
Electrical reservoir capacity				**74.327 MWe**		

Table S9. Result of thermoeconomics analysis of dry steam Asal power plant

Year (t)	ICt ($/kW)	O&Mt ($)	Et (kWh)	PVC ($)
0	3,157.49[1]	0	0	83 125 515.89
1	0	3 734 120.28	155 721 457.14	3 734 120.28
2	0	3 319 218.02	138 419 073.01	3 319 218.02
3	0	2 950 416.02	123 039 176.01	2 950 416.02
4	0	2 622 592.02	109 368 156.45	2 622 592.02
5	0	2 331 192.91	97 216 139.07	2 331 192.91
6	0	2 072 171.47	86 414 345.84	2 072 171.47
7	0	1 841 930.20	76 812 751.86	1 841 930.19
8	0	1 637 271.29	68 278 001.65	1 637 271.29
9	0	1 455 352.25	60 691 557.02	1 455 352.25
10	0	1 293 646.45	53 948 050.69	1 293 646.45
11	0	1 149 907.95	47 953 822.83	1 149 907.95
12	0	1 022 140.40	42 625 620.30	1 022 140.40
13	0	908 569.25	37 889 440.26	908 569.25
14	0	807 617.11	33 679 502.46	807 617.11
15	0	717 881.87	29 937 335.52	717 881.87
16	0	638 117.22	26 610 964.90	638 117.22
17	0	567 215.31	23 654 191.03	567 215.31
18	0	504 191.39	21 025 947.58	504 191.39
19	0	448 170.12	18 689 731.18	448 170.12
20	0	398 373.44	16 613 094.38	398 373.44
21	0	354 109.72	14 767 195.01	354 109.72
22	0	314 764.20	13 126 395.56	314 764.2
23	0	279 790.40	11 667 907.17	279 790.39
24	0	248 702.58	10 371 473.04	248 702.58
25	0	221 068.96	9 219 087.14	221 068.96
Total	3,157.49	**31 838 530.82**	**1 327 740 417.10**	**114 964 046.71**
	LCOE		$cents/KWh	8.66

1. In this subtotal, US$12,964,527 is the drilling cost of one well over a depth of 2500 m at AG rift

Table S10. Result of thermoeconomics analysis of single flash Asal power plant.

Year (t)	ICt ($/kW)	O&Mt ($)	Et (kWh)	PVC ($)
0	3,294.20[1]	0.00	0.00	29 145 684.07
1	0.00	893 677.32	34 423 415.73	893 677.32
2	0.00	794 379.84	30 598 591.76	794 379.84
3	0.00	706 115.41	27 198 748.23	706 115.41
4	0.00	627 658.15	24 176 665.09	627 658.15
5	0.00	557 918.35	21 490 368.97	557 918.35

6	0.00	495 927.42	19 102 550.20	495 927.42
7	0.00	440 824.38	16 980 044.62	440 824.38
8	0.00	391 843.89	15 093 373.00	391 843.89
9	0.00	348 305.68	13 416 331.55	348 305.68
10	0.00	309 605.05	11 925 628.05	309 605.05
11	0.00	275 204.49	10 600 558.26	275 204.49
12	0.00	244 626.21	9 422 718.46	244 626.21
13	0.00	217 445.52	8 375 749.74	217 445.52
14	0.00	193 284.91	7 445 110.88	193 284.91
15	0.00	171 808.81	6 617 876.34	171 808.81
16	0.00	152 718.94	5 882 556.74	152 718.94
17	0.00	135 750.17	5 228 939.33	135 750.17
18	0.00	120 666.82	4 647 946.07	120 666.82
19	0.00	107 259.39	4 131 507.62	107 259.39
20	0.00	95 341.68	3 672 451.22	95 341.68
21	0.00	84 748.16	3 264 401.08	84 748.16
22	0.00	75 331.70	2 901 689.85	75 331.70
23	0.00	66 961.51	2 579 279.87	66 961.51
24	0.00	59 521.34	2 292 693.21	59 521.34
25	0.00	52 907.86	2 037 949.52	52 907.86
Total	3,294.20	**7 619 833.01**	**293 507 145.36**	**36 765 517.08**
	LCOE		$cents/KWh	12.53

1. In this subtotal, US$12,964,527 is the drilling cost of one well over a depth of 2500 m at AG rift

Table S11. Result of Monte Carlo simulation for potential capacity of Asal Well.

Statistics Parameters	Units	Values
Minimum	MWe	6.037
Probability of 5%	MWe	23.462
Probability of 10%	MWe	28.385
Probability of 15%	MWe	32.398
Probability of 20%	MWe	36.060
Probability of 25%	MWe	39.601
Probability of 30%	MWe	43.117
Probability of 32.5%	MWe	44.806
Probability of 35%	MWe	46.657
Probability of 40%	MWe	50.229
Probability of 45%	MWe	53.917
Probability of 50%	MWe	57.729
Probability of 55%	MWe	61.684
Probability of 60%	MWe	65.869
Probability of 65%	MWe	70.368
Probability of 70%	MWe	75.247
Probability of 75%	MWe	80.655
Probability of 80%	MWe	86.849
Probability of 85%	MWe	94.226
Probability of 90%	MWe	103.868

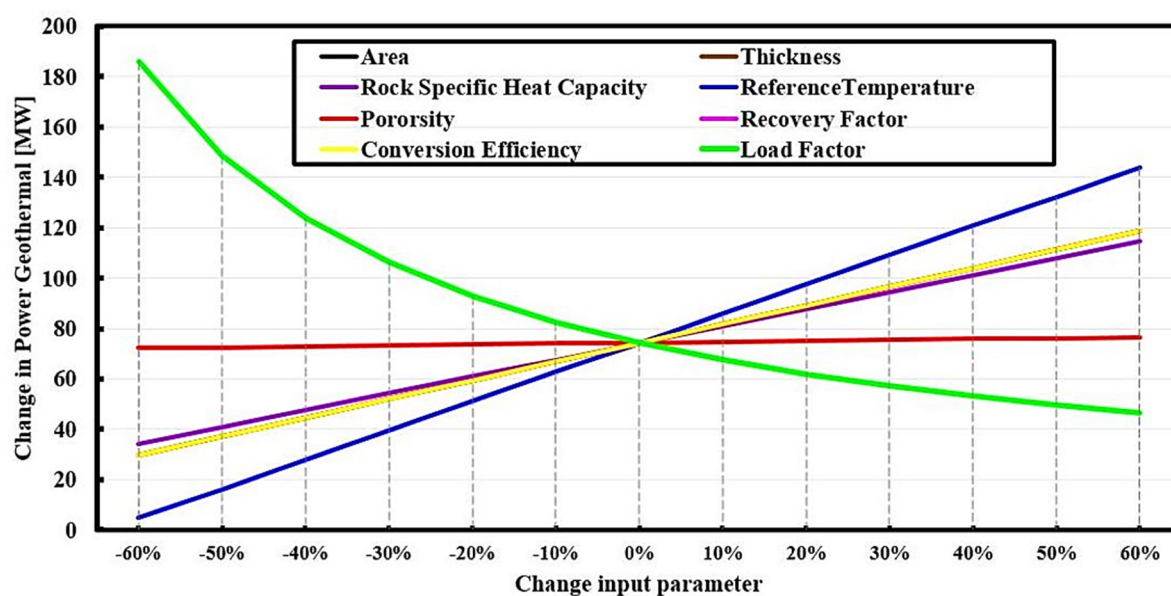| Probability of 95%	MWe	118.800
Average	MWe	62.654
Variance	MWe²	892.33
Standard Deviation	MWe	29.872
Skewness	--	0.847
Kurtosis	--	0.653
Maximum	MWe	241.531
Power density	MWe/km²	8.73
Number of iteration	Times	1,000,000

Figure S11. Sensitivity diagram for volumetric parameters variation.
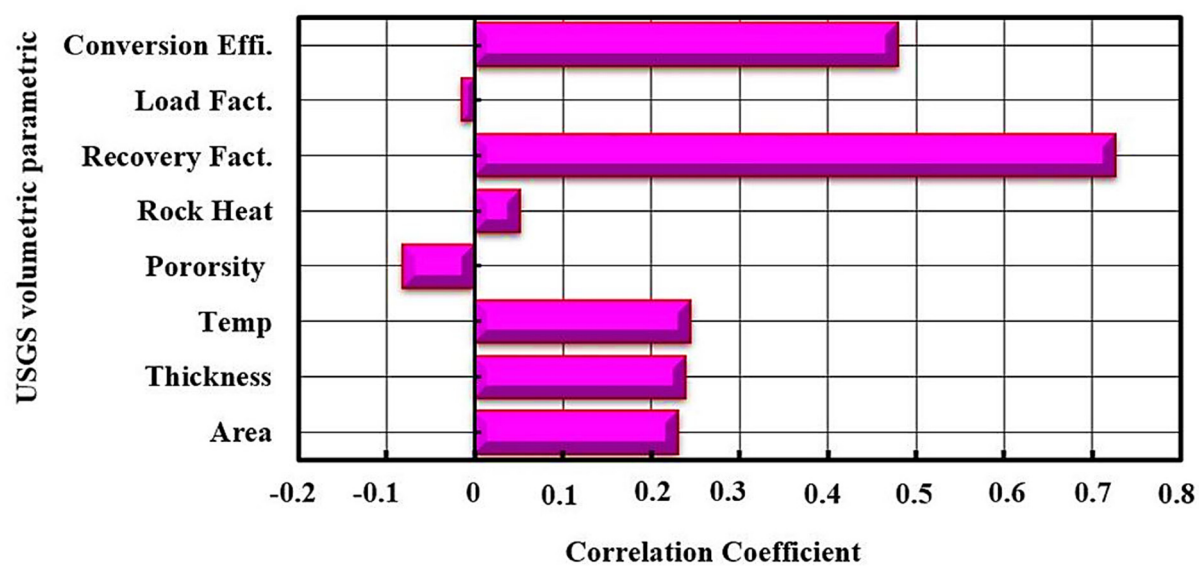
Figure S12. Chart Correlation in Monte Carlo simulation.

Table S12. Result of economic analyses of green hydrogen production supply with the geothermal energy.

Thermodynamic Operation	Electrolyser coupled with geothermal power plant	Total Capital cost (US$)	Electrical cost (US$/year)	Operating and maintenance cost (US$/Year)
Reversible case	Single flash-PEMEm	6527458.79	4850968.83	1033367.94
	Dry steam-PEMEm	21273902.66	15168 751.91	3303587.00
	Single flash-HTE	6919963.95	15168 751.91	1250337.38
	Dry steam-HTE	22732202.50	4850968.83	3997 19.33
Irreversible case	Single flash-PEMEm	5965510.22	4850968.83	712735.56
	Dry steam-PEMEm	19197649.02	15168751.91	2278553.27
	Single flash-HTE	6813861.48	4850968.83	1192163.07
	Dry steam-HTE	22337439.99	15168751.91	3811241.12

The efficiency of the Wind-Electrolyzer system with and without considering degradation rate of wind turbine over the year.

Table S13. Energy efficiency of the wind-powered hydrogen production system in Ghoubbet without and with degradation rate

| yr | Yearly hydrogen production considering different degradation rates (ton/yr) | | | | Input energy (GJ) | Energy efficiency of the examined hydrogen generation system (%) | | | |
| | Without Degradation | | With Degradation | | | Without Degradation | | With Degradation | |
	AWE	PEME	AWE	PEME		AWE	PEME	AWE	PEME
1	398.714	310.111	398.714	310.111		19.802	15.402	19.802	15.402
2	398.714	310.111	392.334	305.149		19.802	15.402	19.486	15.155
3	398.714	310.111	386.057	300.267		19.802	15.402	19.174	14.913
4	398.714	310.111	379.880	295.462		19.802	15.402	18.867	14.674
5	398.714	310.111	373.802	290.735		19.802	15.402	18.565	14.440
6	398.714	310.111	367.821	286.083	285911.89	19.802	15.402	18.268	14.209
7	398.714	310.111	361.936	281.506		19.802	15.402	17.976	13.981
8	398.714	310.111	356.145	277.002		19.802	15.402	17.688	13.757
9	398.714	310.111	350.447	272.570		19.802	15.402	17.405	13.537
10	398.714	310.111	344.840	268.209		19.802	15.402	17.127	13.321
11	398.714	310.111	339.322	263.917		19.802	15.402	16.853	13.108
12	398.714	310.111	333.893	259.695		19.802	15.402	16.583	12.898
13	398.714	310.111	328.551	255.539		19.802	15.402	16.318	12.692
14	398.714	310.111	323.294	251.451		19.802	15.402	16.057	12.488
15	398.714	310.111	318.121	247.428		19.802	15.402	15.800	12.289
16	398.714	310.111	313.031	243.469		19.802	15.402	15.547	12.092
17	398.714	310.111	308.023	239.573		19.802	15.402	15.298	11.899
18	398.714	310.111	303.094	235.740		19.802	15.402	15.053	11.708
19	398.714	310.111	298.245	231.968		19.802	15.402	14.813	11.521
20	398.714	310.111	293.473	228.257		19.802	15.402	14.576	11.337

Table S14. CO_2 and fuel oil avoided with Wind energy development

	Wind CO2 Savings in tonCO2/yr	Wind Barrels Avoided (BA) in bll	Wind CO2 Savings in tonCO2/yr	Wind Barrels Avoided (BA) in bll
	Without Degradation		**With Degradation**	
1	5154.040	11350.051	5154.040	11350.051
2	5154.040	11350.051	5071.575	11168.450
3	5154.040	11350.051	4990.430	10989.755
4	5154.040	11350.051	4910.583	10813.919
5	5154.040	11350.051	4832.014	10640.896
6	5154.040	11350.051	4754.701	10470.642
7	5154.040	11350.051	4678.626	10303.112
8	5154.040	11350.051	4603.768	10138.262
9	5154.040	11350.051	4530.108	9976.050
10	5154.040	11350.051	4457.626	9816.433
11	5154.040	11350.051	4386.304	9659.370
12	5154.040	11350.051	4316.123	9504.820
13	5154.040	11350.051	4247.065	9352.743
14	5154.040	11350.051	4179.112	9203.099
15	5154.040	11350.051	4112.246	9055.850
16	5154.040	11350.051	4046.451	8910.956
17	5154.040	11350.051	3981.707	8768.381
18	5154.040	11350.051	3918.000	8628.087
19	5154.040	11350.051	3855.312	8490.037
20	5154.040	11350.051	3793.627	8354.197

Table S15. Exergoenvironnment of dry steam and single flash power plant

Exergoenvironnment parameter	Unit	Dry steam	Single flash
Toal exergy destruction	KW	18832,08	10813,12
Total input exergy	KW	41052,61	15725,13
impact factor	/	0.46	0.69
Exergy efficiency	%	0.54	0.31
Impact index factor	/	0.85	2.20
Improvement Impact index factor	/	1.18	0.45

References

1. Baseer, M. A.; Meyer, J. P.; Rehman, S.; Alam, M. M. Wind power characteristics of seven data collection sites in Jubail, Saudi Arabia using Weibull parameters. Renewable Energy **2017**, 102, 35–49.

2. Aukitino, T.; Khan, M. M.; Ahmed, M. R. Wind energy resource assessment for Kiribati with a comparison of different methods of determining Weibull parameters. Energy Conversion and Management **2017**, 151, 641–660.

3. Costa Rocha, P. A.; de Sousa, R. C.; de Andrade, C. F.; da Silva, M. V. Comparison of seven numerical methods for determining Weibull parameters for wind energy generation in the northeast region of Brazil. Applied Energy **2012**, 89, 395–400.

4. Tizgui, I.; El Guezar, F.; Bouzahir, H.; Benaid, B. Comparison of methods in estimating Weibull parameters for wind energy applications. International Journal of Energy Sector Management **2017**, 11, 650–663.

5. Wang, J. ; Huang, X. ; Li, Q. ; Ma, X. Comparison of seven methods for determining the optimal statistical distribution parameters: A case study of wind energy assessment in the large-scale wind farms of China. Energy **2018**,164, 432-448.

6. Berretti, S.; Thampi, S. M.; Srivastava, P. R. Intelligent Systems Technologies and Applications. Advances in Intelligent Systems and Computing **2016**, 1.

7. Li, G.; Shi, J. On comparing three artificial neural networks for wind speed forecasting. Applied Energy **2010**, 87, 2313–2320.

8. Ciriaco, A. E.; Zarrouk, S. J.; Zakeri, G. Geothermal resource and reserve assessment methodology: Overview, analysis and future directions. Renewable and Sustainable Energy Reviews **2020**, 119.

9. Muffler, P.; Cataldi, R. Methods for regional assessment of geothermal resources. Geothermics **1978**, 7, 53–89.

10. Pocasangre, C.; Fujimitsu, Y. A. Python-based stochastic library for assessing geothermal power potential using the volumetric method in a liquid-dominated reservoir. Geothermics **2018**, 76, 164–176.

11. Shah, M.; Vaidya, D.; Sircar, A. Using Monte Carlo simulation to estimate geothermal resource in Dholera geothermal field, Gujarat, India. Multiscale and Multidisciplinary Modeling, Experiments and Design **2018**, 1, 83–95.

12. Shamoushaki, M.; Ehyaei, M. A.; Ghanatir, F. Exergy, economic and environmental analysis and multi-objective optimization of a SOFC-GT power plant. Energy **2017**, 134, 515–531.

13. Karapekmez, A.; Dincer, I. Modelling of hydrogen production from hydrogen sulfide in geothermal power plants. International Journal of Hydrogen Energy **2018**, 43, 10569–10579.

14. Darvish, K.; Ehyaei, M.; Atabi, F.; Rosen, M. Selection of Optimum Working Fluid for Organic Rankine Cycles by Exergy and Exergy-Economic Analyses. Sustainability **2015**, 7, 15362–15383.

15. Fallah, M.; Ghiasi, R. A.; Mokarram, N. H. A. Comprehensive comparison among different types of geothermal plants from exergy and thermoeconomic points of view. Thermal Science and Engineering Progress **2018**, 5, 15–24.

16. Staffell, I.; Green, R. How does wind farm performance decline with age? Renewable Energy, **2014** 66, 775–786.

17. Byrne, R.; Astolfi, D.; Castellani, F.; Hewitt, N. A. Study of Wind Turbine Performance Decline with Age through Operation Data Analysis. Energies, **2020**, 13.

18. Hackstein, F. V.; Madlener, R. Sustainable operation of geothermal power plants: why economics matters. Geothermal Energy **2021**, 9, 10.

19. Ortega-Izquierdo, M.; del Río, P. Benefits and costs of renewable electricity in Europe. Renewable and Sustainable Energy Reviews, **2016**, 61, 372–383.

20. Rezaei, M.; Khozani, N.; Jafari, N. Wind energy utilization for hydrogen production in an underdeveloped country: An economic investigation. Renewable Energy **2019**,147, 1044-1057.

21. Shamoushaki, M.; Aliehyaei, M.; Taghizadeh-Hesary, F. Energy, Exergy, Exergoeconomic, and Exergoenvironmental Assessment of Flash-Binary Geothermal Combined Cooling, Heating and Power Cycle. Energies **2021**, 14, 4464.

22. Awaleh, M.O.; Boschetti, T.; Soubaneh, Y.D.; Baudron, P.; Kawalieh, A.D.; Dabar, O.A; Ahmed, M.M.; Ahmed, S.I.; Daoud, M.A.; Egueh, N.M.; Mohamed, J. Geochemical study of the Sakalol-Harralol geothermal field (Republic of Djibouti): Evidences of a low enthalpy aquifer between Manda-Inakir and Asal rift settings. Journal of Volcanology and Geothermal Research, **2017**, 331, 26-52.

23. McPhy Driving Clean Energy Forward. (Accessed on 26 July 2021).

24. Ursua, A.; Gandia, L. M.; and Sanchis, P. Hydrogen Production From Water Electrolysis: Current Status and Future Trends. Proceedings of the IEEE, **2012**, 100, 410–426.

25. Ayodele, T. R.; Munda, J. L. Potential and economic viability of green hydrogen production by water electrolysis using wind energy resources in South Africa. International Journal of Hydrogen Energy **2019**, 44, 17669-16687.

26. Greiner, C.; korpas, M.; Holen, A. A Norwegian case study on the production of hydrogen from wind power. International Journal of Hydrogen Energy **2007**, 32, 1500–1507.

27. Yilmaz, C.; Kanoglu, M.; Bolatturk, A.; Gadalla, M. Economics of hydrogen production and liquefaction by geothermal energy. International Journal of Hydrogen Energy **2012**, 37, 2058–2069.

28. Motazedi, K.; Salkuyeh, Y. K.; Laurenzi, I. J.; MacLean, H. L.; Bergerson, J. A. Economic and environmental competitiveness of high temperature electrolysis for hydrogen production. International Journal of Hydrogen Energy **2021**, 46, 21274–21288.

29. Lucas Bauer and Silvio Matysik. The big portal for wind energy. (Accessed on 25 July 2021).

30. Guangzhou Kai Yuan Water Treatment Equipment Co.Ltd. (Accessed on 26 July 2021).

31. Houssein, D. E.; Axelsson, G. Geothermal resources in the Asal Region, Republic of Djibouti: An update with emphasis on reservoir engineering studies. Geothermics, **2010** 39, 220–227.

32. Halldórsdóttir, S.; Björnsson, H. ; Mortensen, A. ; Axelsson, G.; Guðmundsson. Á. Temperature Model and Volumetric Assessment of the Krafla Geothermal Field in N-Iceland. Proceedings World Geothermal Congress 2010, Bali, Indonesia, **2010**.

33. Gaetan Sakindi. Three-dimensional inversion of magnetotelluric data: geological/geothermal interpretation of Asal geothermal field, Djibouti. Orkustofnun, Grensasvegur 9, IS-108 Reykjavik, Iceland.**2015**.

34. Battistel, A.; RIVERA J.; Ferragina. C. Reservoir Engineering Studies at the Asal Field: Republic of Djibouti. Geothermol Resources Council BUUETlN,**1991**.

35. D'Amore, F.; Giusti, D.; Abdallah, A. Geochemistry of the high-salinity geothermal field of Asal, Republic of Djibouti, Africa. Geothermics, **1998** 27, 197–210.

36. Keilegavlen, E.; Duboeuf, L.; Dichiarante, A. M.; Halldórsdóttir, S.; Stefansson, I.; Naumann, M.; Berre, I. Hydro-mechanical simulation and analysis of induced seismicity for a hydraulic stimulation test at the Reykjanes geothermal field, Iceland. Geothermics **2021**, 97, 102223.

37. Juncu, D.; Árnadóttir, T.; Geirsson, H.; Gunnarsson, G. The effect of fluid compressibility and elastic rock properties on deformation of geothermal reservoirs. Geophysical Journal International, **2019**, 217, 122–134.

38. Keiding, M.; Árnadóttir, T.; Jónsson, S.; Decriem, J.; Hooper, A. Plate boundary de formation and man-made subsidence around geothermal fields on the Reykjanes Peninsula, Iceland. Journal of Volcanology and Geothermal Research **2010**, 194, 139–149.

39. Jacoby, W. R.; Weigel, W.; Fedorova, T. Crustal structure of the Reykjanes Ridge near 62°N, on the basis of seismicre fraction and gravity data. Journal of Geodynamics, **2007**, 43, 55–72.

40. Cornel O. An update of the natural state numerical model of olkaria geothermal system, kenya. Proceedings, Tough symposium 2003 Lawrence Berkeley National Laboratory, Berkeley, California, **2003**.

41. Hochstein, M. P. Comments on: The structure of the shallow crust beneath Olkaria geothermal field, Kenya, deduced from gravity studies, by J.M. Ndombi. Journal, **1984**.

42. Nadimi, S.; Forbes, B.; Moore, J.; Podgorney, R.; McLennan, J. D. Utah FORGE: Hydrogeothermal modeling of agranitic based discrete fracture network. Geothermics, **2020**, 87, 101853.

43. Fauzi, A. Geothermal resources and reserves in Indonesia: an updatedrevision. Geoth. Energ. Sci. **2015**, 3, 1–6.

44. Banks, J.; Harris, N. B. Geothermal potential of Foreland Basins: A case study from the Western Canadian Sedimentary Basin. Geothermics, **2018**, 76, 74–92.

45. Júlíusson, E.; Axelsson, G. Stock models for geothermal resources. Geothermics, **2018**, 72, 249–257.

46. Garg, S. K.; Combs, J. A reformulation of USGS volumetric "heat in place" resource estimation method. Geothermics **2015**, 55, 150–158.

47. Virkir-Orkint Consulting Group Ltd. Geothermal scaling and corrosion study, final report, Djibouti.Reykjanik, Iceland, August, **1990**.

48. Gaucher, E.T.; Kohl, F.; Limberger, A. ; Dimier, J. Wang. Wellbore Simulator Application to RN-15/IDDP-2 well (Reykjanes, Iceland). DEEPEGS.**2015**.